Chin. J. Astron. Astrophys. Vol. 3 (2003), No. 3, 191–202
(http://www.chjaa.org or http://chjaa.bao.ac.cn)

Chinese Journal of Astronomy and Astrophysics

Resolved SZE Cluster Count

Jia-Yu Tang [1] and Zu-Hui Fan [1,2]

[1] Department of Astronomy, Peking University, Beijing 100871; tangjy@vega.bac.pku.edu.cn
[2] Chinese Academy of Sciences-Peking University Joint Beijing Astrophysics Center, Beijing 100871

Received 2002 December 21; accepted 2003 April 1

Abstract We study the counts of resolved SZE (Sunyaev-Zel'dovich effect) clusters expected from an interferometric survey in different cosmological models under different conditions. The self-similar universal gas model and Press-Schechter mass function are used. We take the observing frequency to be 90 GHz, and consider two dish diameters, 1.2 m and 2.5 m. We calculate the number density of the galaxy clusters $\mathrm{d}N/(\mathrm{d}\Omega \mathrm{d}z)$ at a high flux limit $S_\nu^{\lim} = 100\,\mathrm{mJy}$ and at a relative low $S_\nu^{\lim} = 10\,\mathrm{mJy}$. The total numbers of SZE clusters N in two low-Ω_0 models are compared. The results show that the influence of the resolved effect depends not only on D, but also on $S_\nu^{\lim}$: at a given D, the effect is more significant for a high than for a low $S_\nu^{\lim}$. Also, the resolved effect for a flat universe is more impressive than that for an open universe. For $D = 1.2\,\mathrm{m}$ and $S_\nu^{\lim} = 10\,\mathrm{mJy}$, the resolved effect is very weak. Considering the designed interferometers which will be used to survey SZE clusters, we find that the resolved effect is insignificant when estimating the expected yield of the SZE cluster surveys.

Key words: cosmology: theory — galaxy: cluster: general —large-scale structure of universe

1 INTRODUCTION

Galaxy clusters, the largest virialized objects in the universe, consist of hundreds to thousands of galaxies: they are the molecules of our huge universe. They represent structures on scales of Mpc. Through the study of galaxy clusters, we can find much valuable information on structure formation and cosmology. Especially, statistical investigation of large samples of such clusters can constrain the fundamental cosmological parameters and thus distinguish different cosmology models.

Nowadays, many observational approaches are used to survey and to study the clusters, such as strong and weak gravitational lensing, X-ray and optical observations. During the last 10 years, interferometric techniques have been developed significantly, making it possible to survey the clusters by detecting their Sunyaev-Zel'dovich effect (e.g., Bartlett 2000; Carlstrom et al. 2000; Kneissl et al. 2001, hereafter the SZ effect).

The SZ effect is generated through the interaction of intracluster hot electrons with cosmic microwave background (CMB) photons (Sunyaev & Zel'dovich 1980). A cluster of galaxies consists of a dark matter halo, galaxies and a hot intracluster medium (ICM). The typical temperature of the ICM is $10^7 - 10^8$ K. Galaxies and hot gas are in dynamical equilibrium with the potential well of the dark matter halo. When CMB photons pass through the cluster, their distribution of frequency changes due to the inverse Compton scattering with the hot electrons. As a result, the CMB intensity is increased at frequencies $\nu > 219$ GHz and is decreased at frequencies $\nu < 219$ GHz. The equivalent temperature increment (or decrement) ΔT of the CMB photons toward a cluster is proportional to $\int n_{\rm e} T_{\rm gas} {\rm d}l$, where $n_{\rm e}$ is the number density of the electrons, $T_{\rm gas}$ is the temperature of the hot gas, and ${\rm d}l$ is the line element along the line of sight. The temperature change ΔT, depending only on the thermal energy of the scattering hot electrons which is determined by the mass of galaxy clusters, is redshift independent.

In the standard picture of structure formation, the growth of density perturbations depends on the cosmological model, especially on the density parameter Ω_0. Therefore when normalized to the local cluster abundance, the redshift distribution of cluster abundance would be very different for different models. Thus observation on the redshift distribution places useful constraints on cosmological parameters (e.g., Bahcall & Fan 1998; Fan & Chiueh 2001; Oukbir et al. 1997; Viana & Liddle 1999). As the distribution at high redshift is the part most sensitive to cosmological models, SZE cluster survey is very ideal in this regard.

A few authors (e.g., Barbosa et al. 1996; Bartlett 2000; Holder et al. 2000; Kneissl et al. 2000) have calculated the redshift distribution of the number density of clusters expected from a SZE survey. Much of their work concentrated on unresolved SZE clusters or assessed the resolved effects with mock surveys. In this paper, we study the resolved effect on SZE cluster counts expected from an interferometric survey systematically with an analytical approach. For an interferometric survey, there is a minimum baseline essentially limited by the dish diameter D, which corresponds to the cutoff angular scale $\theta_{\rm c} = \lambda/(2D)$. When $\theta_{\rm c}$ is larger than the angular scale of a cluster, all the SZE signal from the cluster will be received by the interferometer; otherwise, part of the SZE signal will be lost. To address this, we use the self-similar gas model (Komatsu & Seljak 2001) to describe the gas density profile. The Press-Schechter function is used to calculate the number density of SZE clusters analytically.

The rest of the paper is organized as follows. In Section 2 we determine the minimum observable cluster mass $M_{\rm lim}(z)$ given $S_\nu^{\rm lim}$. In Section 3 the number densities of resolved SZE clusters in different cosmological models are calculated and in Section 4 we give a discussion.

2 DETERMINATION OF MASS THRESHOLD

We begin this section by calculating the SZE flux and in subsection 2.2 we study the profile of the intracluster gas and detail how to determine the mass thresholds under different conditions.

2.1 SZE Flux

The electron temperature $T_{\rm gas}$ in the ICM is much higher than the CMB photon temperature $T_{\rm CMB}$ and $kT_{\rm gas}/(m_{\rm e}c^2) \ll 1$, the change of the CMB intensity due to the inverse-Compton scattering can be written as (Sunyaev & Zel'dovich 1980)

$$\frac{\Delta I}{I_{\rm CMB}} = Q(x) y \ , \tag{1}$$

where $x = h_p\nu/kT_{\rm CMB}$, ν is the frequency of the CMB photons, h_p is the Planck constant, $Q(x)$ has the form

$$Q(x) = \frac{xe^x}{e^x - 1}\Big[\ \frac{x}{\tanh(x/2)} - 4\ \Big], \tag{2}$$

and

$$y = \int n_{\rm e}\sigma_{\rm T}\frac{kT_{\rm gas}}{m_{\rm e}c^2}{\rm d}l \tag{3}$$

is the Compton parameter, where $n_{\rm e}$ is the number density of hot electrons, $\sigma_{\rm T} = 6.65 \times 10^{-25}{\rm cm}^2$ is the Thomson cross section, k is the Boltzmann constant, $T_{\rm gas}$ is the temperature of the intracluster hot gas, $m_{\rm e}$ is the electron mass, and c is the speed of light. Then the SZE flux can be calculated as

$$S_\nu = S_\nu^{\rm CMB}\int\frac{\Delta I}{I_{\rm CMB}}{\rm d}\Omega = S_\nu^{\rm CMB}Q(x)\int y{\rm d}\Omega = S_\nu^{\rm CMB}Q(x)Y, \tag{4}$$

where $Y = \int y{\rm d}\Omega = \int ydA/R_d^2$, R_d is the angular diameter distance, and $S_\nu^{\rm CMB} = (2h_p\nu^3/c^2)/(e^x - 1)$ represents the unperturbed CMB specific intensity.

We assume that the intracluster gas is spherical and isothermal and the gas mass fraction $f_{\rm ICM}$ is a constant. Then, for the unresolved case, i.e., if the cutoff angle is large enough that the full SZE signal can be received by the interferometer, the integral in Eq.(4) is taken over the projected area of the whole cluster,

$$Y = \frac{\sigma_{\rm T}}{2m_{\rm e}m_{\rm p}c^2}R_d^{-2}f_{\rm ICM}(1+X)kT_{\rm gas}M_{\rm vir}, \tag{5}$$

where $m_{\rm p}$ is the proton mass, X is the hydrogen mass fraction, and $M_{\rm vir}$ is the virial mass of the cluster. Then

$$\begin{aligned} S_\nu \ =\ & 2.29\times10^4\frac{x^3}{e^x-1}Q(x)\times1.70\times10^{-2}h\Big(\frac{f_{\rm ICM}}{0.1}\Big)\Big(\frac{1+X}{1.76}\Big) \\ & \times\frac{7.75}{0.5[{\rm d}\ln\rho_{\rm gas}(r)/{\rm d}\ln r]_{r_{\rm vir}}}\Big(\frac{6.8}{5X+3}\Big)\Big(\frac{R_d}{100\,h^{-1}\,{\rm pc}}\Big)^{-2} \\ & \times(1+z)\Big[\ \frac{\Omega_0}{\Omega(z)}\ \Big]^{1/3}\Big(\frac{\Delta_c}{178}\Big)^{1/3}\Big(\frac{M_{\rm vir}}{10^{15}\,h^{-1}\,M_\odot}\Big)^{5/3}{\rm mJy}, \end{aligned} \tag{6}$$

where $1\,{\rm mJy}=10^{-26}$ erg cm^{-2} s^{-1} Hz^{-1}, h is the Hubble constant in units of $100\,{\rm km\ s^{-1}\ Mpc^{-1}}$, $\Omega(z)$ is the density parameter at redshift z, $\rho_{\rm gas}(r)$ is the radial density profile of the gas, $r_{\rm vir}$ stands for the virial radius of the cluster, and Δ_c is the average mass density with respect to the critical density at redshift z of the cluster formation (Fan & Chiueh 2001). Here the hydrostatic equilibrium condition has been used in relating $T_{\rm gas}$ to $M_{\rm vir}$, which will be given in Eq.(16).

However, for an array of interferometers, there exists a minimum baseline which is essentially limited by the dish diameter D. Then, signals from angular scales larger than $\lambda/2D$ are lost (λ the observing wavelength). As a result, the integral in Eq.(4) is taken over the projected area with $\theta \le \theta_{\rm c}$ and the results depend on the mass of gas contained in this region. Therefore, the observed SZE flux depends on the density profile of the intracluster gas if θ_c is significantly less than the angular scale of a cluster.

2.2 The Gas Profile

So far, the isothermal β-model is the most popular model for calculating the gas density profile (Birkinshaw 1999). It consists of a central core and a power law outer part with slope β:

$$\rho_{\rm gas}(r) = \rho_{\rm gas}(0)\Big[1 + \Big(\frac{r}{r_{\rm c}}\Big)^2\Big]^{-3\beta/2}, \tag{7}$$

where $r_{\rm c}$ is the core radius. Though this model fits well the X-ray emissions which are mainly from the central parts of clusters, it becomes less accurate for the outskirts of the gas distribution, where the SZ effects are still relatively significant. In the following we will describe the self-similar gas density profile (Komatsu & Seljak 2001), which is based on the assumption of hydrostatic equilibrium and on that the gas density profile traces the dark matter density profile in the outer part of a halo.

N-body simulations suggest that a dark matter halo has a self-similar density profile (Navarro, Frenk & White 1997; Komatsu & Seljak 2001)

$$\rho_{\rm DM} = \rho_s y_{\rm DM}(r/r_s), \tag{8}$$

where ρ_s is a normalization factor of mass density, $y_{\rm DM}$ is a dimensionless function representing the dark matter density profile, r_s is the characteristic scale that separates the inner and outer parts of the profile.

Following usual convention, we define the concentration parameter c as

$$c \equiv r_{\rm vir}/r_s, \tag{9}$$

where the virial radius $r_{\rm vir}$ can be calculated according to (e.g., Peebles 1980)

$$r_{\rm vir} = \Big[\ \frac{M_{\rm vir}}{(4\pi/3)\rho_c(z)\Delta_c(z)}\ \Big]^{1/3}. \tag{10}$$

Then from Eq.(8), we have

$$M_{\rm vir} = 4\pi\rho_s c^{-3} r_{\rm vir}^3 m(c)\ , \tag{11}$$

where $m(x)$ is defined as

$$m(x) = \int_0^x u^2 y_{\rm DM}(u){\rm d}u\ . \tag{12}$$

Makino et al. (1998) and Suto et al. (1998) suggested that hydrostatic equilibrium between the gas pressure and the self-similar dark matter eventually gives the self-similar gas density profile as

$$\rho_{\rm gas}(r) = \rho_{\rm gas}(0) y_{\rm gas}(r/r_s), \tag{13}$$

where $\rho_{\rm gas}(0)$ is the gas density at $r = 0$, $y_{\rm gas}(r/r_s)$ is the normalized gas density profile. In the following, we give a detailed derivation for the isothermal case. The hydrostatic equilibrium condition indicates

$$\rho_{\rm gas}^{-1}\frac{{\rm d}P_{\rm gas}}{{\rm d}r} = -G\frac{M(\le r)}{r^2}, \tag{14}$$

where G is the gravitational constant, $M(\le r)$ is the dark matter mass enclosed in radius r. With $P_{\rm gas} = kn_{\rm gas}T_{\rm gas}$ and $T_{\rm gas}$ a constant, we have

$$\frac{kT_{\rm gas}}{\mu_{\rm gas}m_{\rm p}}\frac{{\rm d}\ln\rho_{\rm gas}}{{\rm d}r} = -G\frac{M(\le r)}{r^2}, \tag{15}$$

where $\mu_{\rm gas} = 4/(5X+3)$ is the mean molecular weight. Taking $r = r_{\rm vir}$, we obtain

$$kT_{\rm gas} = -\frac{1}{[{\rm d}\ln\rho_{\rm gas}(r)/{\rm d}\ln r]_{r_{\rm vir}}}\mu_{\rm gas}m_{\rm p}\frac{GM_{\rm vir}}{r_{\rm vir}}, \tag{16}$$

where $[{\rm d}\ln\rho_{\rm gas}(r)/{\rm d}\ln r]_{r_{\rm vir}}$ can be obtained from Komatsu & Seljak (2001). Substituting $M(\leq r)$ in Eq.(15) for Table A1 (see Appendix), we have

$$\ln\left[\frac{\rho_{\rm gas}(r)}{\rho_{\rm gas}(0)}\right] = \left[\frac{{\rm d}\ln\rho_{\rm gas}(r)}{{\rm d}\ln r}\right]_{r_{\rm vir}} \times \frac{c}{m(c)}\int_0^x \frac{m(u)}{u^2}{\rm d}u\ , \tag{17}$$

where $x = c \times r/r_{\rm vir}$. Comparing Eq. (17) with Eq. (13), we find

$$y_{\rm gas}(x) = \exp\left\{\left[\frac{{\rm d}\ln\rho_{\rm gas}(r)}{{\rm d}\ln r}\right]_{r_{\rm vir}} \times \frac{c}{m(c)}\int_0^x \frac{m(u)}{u^2}{\rm d}u\right\}. \tag{18}$$

We adopt

$$y_{\rm DM} = \frac{1}{x^{\alpha}(1+x)^{3-\alpha}}, \tag{19}$$

the most common form used in N−body simulations, to calculate the gas density profile, where α is a parameter which is often taken as 1.0 (Navarro et al. 1997) or 1.5 (Moore et al. 1998; Jing & Suto 2000). In this paper, we take $\alpha = 1.0$. The other useful formulae are listed in Table A1. We plot $y_{\rm gas}$ for different masses ($10^{13}h^{-1}M_{\odot}$, $10^{14}h^{-1}M_{\odot}$, $10^{15}h^{-1}M_{\odot}$), in Fig. 1.

When the cutoff angular scale $\theta_{\rm c}$ is less than the angular radius of the cluster, then

$$\begin{aligned} Y &= \int y{\rm d}\Omega = R_d^{-2}\int y{\rm d}A = R_d^{-2}\int_0^{r_{\rm lim}} 2\pi r\int n_e\sigma_{\rm T}\frac{kT_{\rm gas}}{m_{\rm e}c^2}{\rm d}l{\rm d}r = \frac{\sigma_{\rm T}}{2m_{\rm e}m_{\rm p}c^2}R_d^{-2}f_{\rm ICM} \\ &\times(1+X)kT_{\rm gas}M_{\rm vir}\frac{2\pi\int_0^{r_{\rm lim}} r(\int\rho_{\rm gas}(\sqrt{r^2+l^2}){\rm d}l){\rm d}r}{\int_0^{r_{\rm vir}}4\pi r^2\rho_{\rm gas}(r){\rm d}r}, \end{aligned} \tag{20}$$

where $r_{\rm lim} = \theta_{\rm c} \times R_d$ is the radius of the field that the interferometer can see at redshift z.

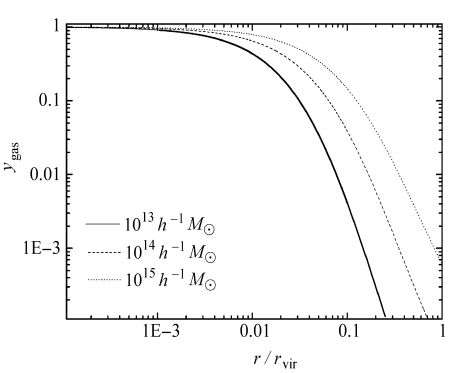

Fig. 1 Normalized density profile of the intracluster gas. The mass above every curve represents the virial mass of the cluster.

Then, the resolved SZE flux can be calculated as

$$
\begin{aligned}
S_\nu \;=\; & 2.29\times10^4\frac{x^3}{e^x-1}Q(x)\times1.70\times10^{-2}h\times\Big(\frac{f_{\rm ICM}}{0.1}\Big)\Big(\frac{1+X}{1.76}\Big)\\
&\times\frac{7.75}{0.5[{\rm d}\ln\rho_{\rm gas}(r)/{\rm d}\ln r]_{\rm vir}}\Big(\frac{6.8}{5X+3}\Big)\Big(\frac{R_d}{100h^{-1}{\rm Mpc}}\Big)^{-2}\\
&\times(1+z)\Big[\;\frac{\Omega_0}{\Omega(z)}\;\Big]^{\frac{1}{3}}\Big(\frac{\Delta_c}{178}\Big)^{\frac{1}{3}}\Big(\frac{M_{\rm vir}}{10^{15}h^{-1}M_\odot}\Big)^{\frac{5}{3}}\\
&\times\frac{2\pi\int_0^{r_{\rm lim}}r(\int\rho_{\rm gas}(\sqrt{r^2+l^2}){\rm d}l){\rm d}r}{\int_0^{r_{\rm vir}}4\pi r^2\rho_{\rm gas}(r){\rm d}r}\,{\rm mJy}.
\end{aligned}
\tag{21}
$$

We see that given the cutoff angular scale and the redshift, the SZE flux decreases with decreasing $M_{\rm vir}$. Then for a given flux limit, there is a minimum mass for a cluster to be observable. In our calculation, we take the observational frequency $\nu = 90\,{\rm GHz}$ and the dish diameter as 1.2 m and 2.5 m. Then $\lambda \simeq 0.33\,{\rm cm}$, and $\lambda/2D \sim 2.27$ arcmin for $D = 2.5\,{\rm m}$ and $\lambda/2D \sim 4.7$ arcmin for $D = 1.2\,{\rm m}$. For a given flux limit $S_\nu^{\rm lim}$, $M_{\rm lim}(z)$ can be obtained from Eq.(21).

Four different cosmological models are considered here:

- SCDM: $\Omega_0 = 1.0, \Omega_\Lambda = 0, h = 0.5, \Gamma = 0.5, \sigma_8 = 0.52$;
- τ-CDM: $\Omega_0 = 1.0, \Omega_\Lambda = 0, h = 0.5, \Gamma = 0.25, \sigma_8 = 0.52$;
- open-CDM: $\Omega_0 = 0.3, \Omega_\Lambda = 0, h = 0.83, \Gamma = 0.25, \sigma_8 = 0.87$;
- ΛCDM: $\Omega_0 = 0.3, \Omega_\Lambda = 0.7, h = 0.83, \Gamma = 0.25, \sigma_8 = 0.93$;

where Γ is the shape parameter of the power spectrum of the linear density fluctuation, and σ_8 is the rms fluctuation amplitude smoothed over $8h^{-1}$ Mpc.

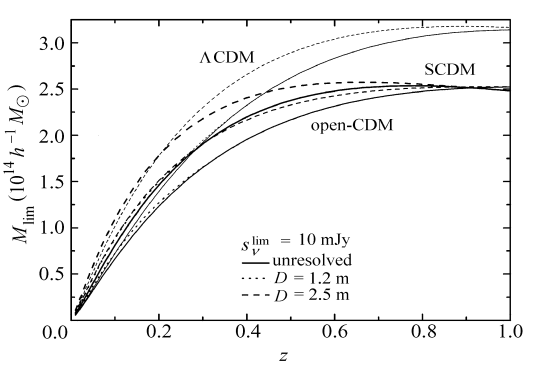

Fig. 2 $M_{\rm lim}(z)$ with $S_\nu^{\rm lim} = 10\,{\rm mJy}$. The thick line is for SCDM model, the thinner for open-CDM model and the thinnest for ΛCDM, respectively. The solid line represents the unresolved case and the dotted line for $D = 1.2\,{\rm m}$ and the dash for $D = 2.5\,{\rm m}$, respectively. Because the resolved effect for $D = 1.2\,{\rm m}$ is very small, the dotted lines are little different from the solid lines and are barely recognizable.

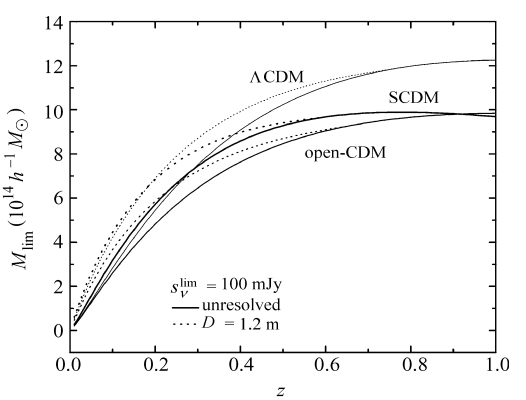

Fig. 3 $M_{\rm lim}(z)$ with $S_\nu^{\rm lim} = 100\,{\rm mJy}$. The thick line is for SCDM model, the thinner for open-CDM model and the thinnest for ΛCDM, respectively. The solid line represents the unresolved case and the dotted line for $D = 1.2\,{\rm m}$, respectively.

Figure 2 shows $M_{\rm lim}(z)$ for $S_\nu^{\rm lim} = 10$ mJy. The thick lines represent the mass threshold for SCDM model and τ-CDM model (from Eqs.(6) and (21), we find that Γ is irrelevant here, so the result for the SCDM model is the same as for the τ-CDM model). The thinner lines represent the mass threshold for the open-CDM model and the thinnest lines for the ΛCDM. The solid lines plot the unresolved results, the dotted lines plot the results for $D = 1.2\,$m and the dash lines for $D = 2.5\,$m. We see that the resolved effect for $D = 1.2\,$m is very small. We show $M_{\rm lim}(z)$ for $S_\nu^{\rm lim} = 100$ mJy in Fig. 3. The line types are all the same as Fig. 2. It is notable that given $D = 1.2\,$m, the resolved effect for $S_\nu^{\rm lim} = 100$ mJy is much stronger than that for $S_\nu^{\rm lim} = 10$ mJy.

3 SZE CLUSTER COUNT

Given $M_{\rm lim}(z)$, the number density ${\rm d}N/({\rm d}\Omega{\rm d}z)$ of clusters with masses $M_{\rm vir} > M_{\rm lim}$ can be obtained by

$$\begin{aligned}\frac{{\rm d}N}{{\rm d}\Omega{\rm d}z} &= \frac{{\rm d}V}{{\rm d}\Omega{\rm d}z}\int_{M_{\rm lim}(z)} n(M){\rm d}M \\ &= \frac{c}{H_0}R_d^2\Big[\,\frac{\Omega_0}{1+z}+\Big(\frac{\Omega_\Lambda}{1+z}\Big)^4+\Big(\frac{\Omega_k}{1+z}\Big)^2\,\Big]^{-\frac{1}{2}}\times\int_{M_{\rm lim}(z)}^{\infty} n(M,z){\rm d}M, \qquad (22)\end{aligned}$$

where $n(M,z)$ is the comoving number density of clusters between masses M and $M+dM$ at redshift z. According to Press & Schechter (1974),

$$n(M,z) = -\Big(\frac{2}{\pi}\Big)^{\frac{1}{2}}\frac{\rho_0}{M}\frac{\delta_c(z)}{\sigma_0^2}\frac{{\rm d}\sigma_0}{{\rm d}M}\exp\Big[-\frac{\delta_c^2(z)}{2\sigma_0^2}\Big], \qquad (23)$$

where ρ_0 is the present mean cosmic mass density, σ_0 the variance of linear fluctuations smoothed over the mass scale M at the present time, and $\delta_c(z)$ the threshold of the linear overdensity of a perturbation which has collapsed and virialized at redshift z. We take $\delta_c(z)/\sigma_0$ as (Navarro et al. 1997; Jain & Seljak 1997)

$$\frac{\delta_c(z)}{\sigma_0} = \frac{\delta_c^0(\Omega(z))}{D_+(z,\Omega_0,\Lambda)\sigma_8(\frac{R}{8h^{-1}{\rm Mpc}})^{-\gamma(R)}}, \qquad (24)$$

where $D_+(z,\Omega_0,\Lambda)$ is the linear growth factor, and following Holder et al. (2000),

$$\gamma(R) = (0.3\Gamma+0.2)\Big[2.92+\log_{10}\Big(\frac{R}{8h^{-1}{\rm Mpc}}\Big)\Big]. \qquad (25)$$

The comoving radius R is determined through

$$R = \Big(\frac{M}{\frac{4\pi}{3}\rho_0}\Big)^{\frac{1}{3}} = 9.5084h^{-1}\Big(\frac{M}{10^{15}h^{-1}M_\odot\Omega_0}\Big)^{\frac{1}{3}}{\rm Mpc}. \qquad (26)$$

Combining Eqs.(23), (24), (25) and (26), we can obtain

$$\begin{aligned}n(M,z)dM &= 2.5139\times10^{-31}h^3\Omega_0\Big(\frac{M}{10^{15}h^{-1}M_\odot}\Big)^{-2}\times\frac{\delta_c(z)}{\sigma_0}\times\Big[(0.3\Gamma+0.2) \\ &\quad\times\log_{10}\Big(\frac{R}{8h^{-1}{\rm Mpc}}\Big)+\gamma(R)\Big]\exp\Big(-\frac{\delta_c^2(z)}{2\sigma_0^2}\Big){\rm d}\Big(\frac{M}{10^{15}h^{-1}M_\odot}\Big). \qquad (27)\end{aligned}$$

4 RESULT AND DISCUSSION

Using Eqs.(22), (27) and $M_{\rm lim}(z)$ derived before, we calculate $\mathrm{d}N/(\mathrm{d}\Omega \mathrm{d}z)$ for four cosmological models and the total number of SZE clusters in the two low-Ω_0 models listed in Section 2.2.

The SZE cluster distributions are shown in Fig. 4 with $S_\nu^{\rm lim} = 10\,$mJy and in Fig. 5 with $S_\nu^{\rm lim} = 100$ mJy. It can be seen that in the unresolved cases, the curves with $\Omega_0 = 1$ are drastically different from those of the low-Ω_0 models, while the differences between the two low-Ω_0 models are not impressive, especially for $S_\nu^{\rm lim} = 100$ mJy. However, for $S_\nu^{\rm lim} = 10$ mJy, it is still possible to distinguish the ΛCDM model from the open-CDM model, because the curve of the latter has a long tail at high redshift (Fan & Chiueh 2001). Moreover, the expected resolved number densities of galaxy clusters are lower than the unresolved ones. We can also find that the redshift distribution of $\Omega_0 = 1$ models is still drastically different from that of low-Ω_0 models, but the differences between the two low-Ω_0 models are sensitive to the resolved effect. In the following, we mainly discuss the influence of the resolved effect on the two low-Ω_0 cosmological models.

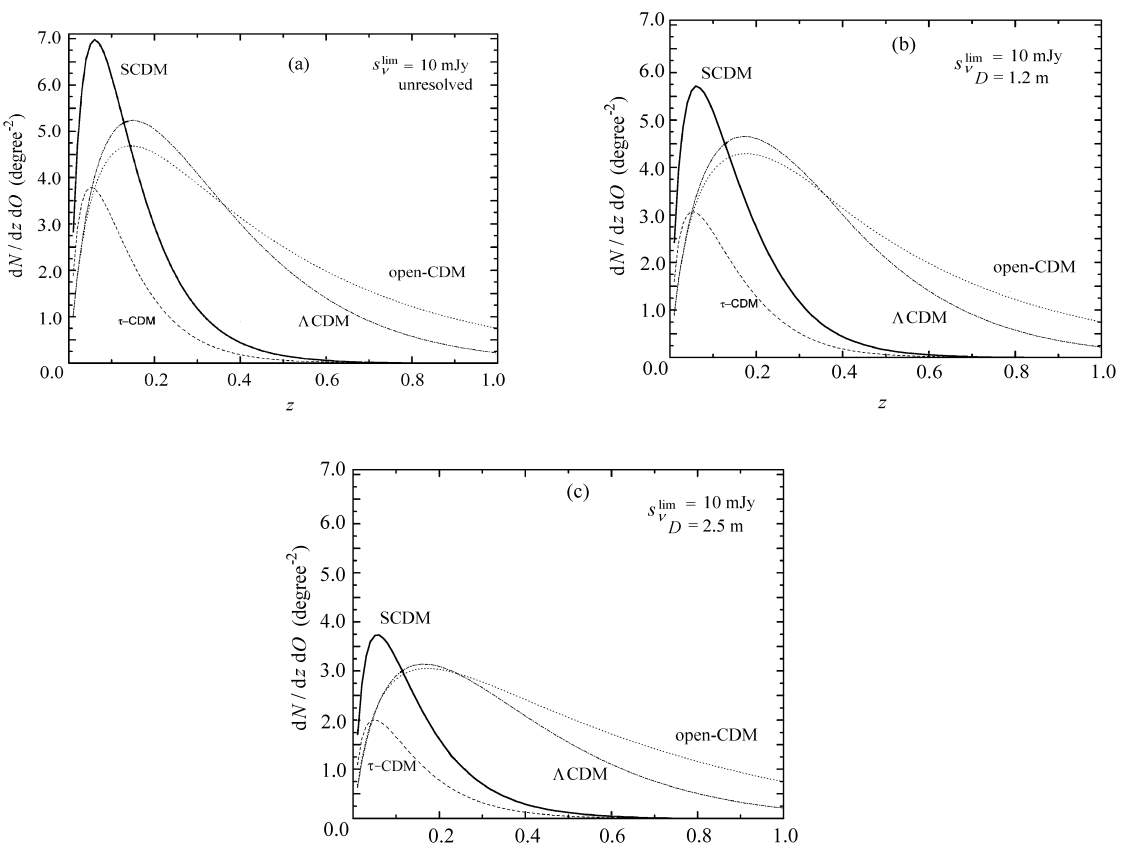

Fig. 4 Redshift distribution of SZE clusters with $S_\nu^{\rm lim} = 10\,$mJy. The solid, dash, dotted and dash−dotted line represent SCDM, τ-CDM, open−CDM and ΛCDM, respectively. Fig. 4 (a), (b), (c) represent the unresolved case, and the cases with $D = 1.2\,$m and $D = 2.5\,$m.

It can be seen clearly that the resolved effect increases with increasing D or $S_\nu^{\rm lim}$, and that, for the same parameter values, the influence of the resolved effect for the ΛCDM model is more significant than that for the open model.

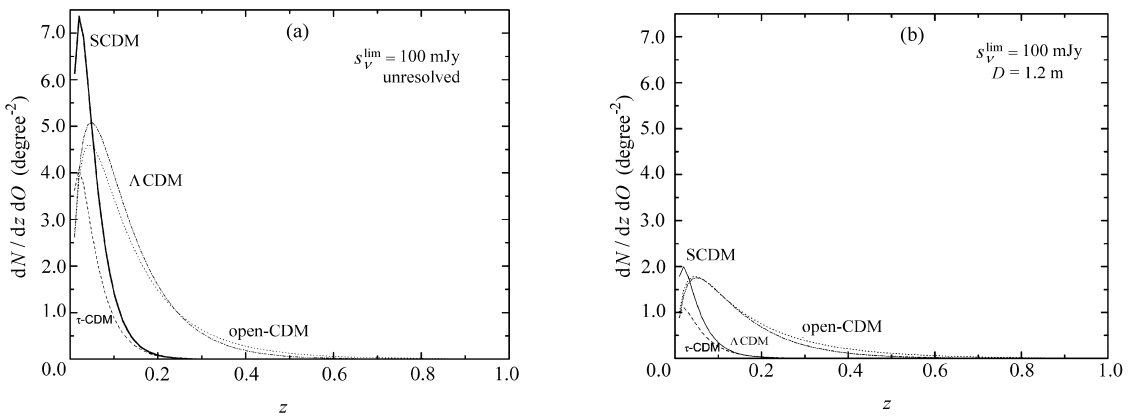

Fig. 5 Redshift distribution of SZE clusters with $S_\nu^{\rm lim} = 100\,{\rm mJy}$. The solid, dash, dotted and dash−dotted line represent the SCDM, τ-CDM, open−CDM and ΛCDM, respectively. Fig. 5 (a) and (b) represent the unresolved case and the case with $D = 1.2\,{\rm m}$, respectively.

The resolved effect changes the mass threshold function from Eqs.(6) to (21) through multiplying the right side of Eq. (6) by $\frac{2\pi\int_0^{r_{\rm lim}} r(\int \rho_{\rm gas}(\sqrt{r^2+l^2}){\rm d}l){\rm d}r}{\int_0^{r_{\rm vir}} 4\pi r^2\rho_{\rm gas}(r){\rm d}r}$, which can be rewritten as

$$F(z, x'_{\rm lim}) = \frac{2\pi\int_0^{x'_{\rm lim}} x'[\int y_{\rm gas}(c\sqrt{x'^2 + (\frac{l}{r_{\rm vir}})^2}){\rm d}(\frac{l}{r_{\rm vir}})]{\rm d}x'}{\int_0^1 4\pi x'^2 y_{\rm gas}(cx'){\rm d}x'}, \tag{28}$$

where $x' = r/r_{\rm vir}$ is the dimensionless radius of the galaxy clusters, $x'_{\rm lim} = r_{\rm lim}/r_{\rm vir}$ represents the radius of the area that the interferometer can see. Therefore, $F(z, x'_{\rm lim})$ denotes the influence of the resolved effect. In fact, $F(z, x'_{\rm lim})$ is the ratio of the projected gas mass contained in $r_{\rm lim}$ to the total gas mass in a galaxy cluster. Obviously, $F(z, x'_{\rm lim})$ increases with increasing $x'_{\rm lim}$. According to our definition,

$$x'_{\rm lim} = \frac{r_{\rm lim}}{r_{\rm vir}} \propto \frac{R_d/D}{[M_{\rm vir}/(\rho_c(z)\Delta_c(z))]^{1/3}} \tag{29}$$

is dependent on the cosmological parameters, the dish diameter D, the redshift z and $M_{\rm vir}$. Given z, the cosmological model and $M_{\rm vir}$, $x'_{\rm lim}$ decreases with increasing D. So, the resolved effect will be stronger with an increase in D.

Given D and $S_\nu^{\rm lim}$, it is also derived that

$$\frac{[x'_{\rm lim}]_{\rm open}}{[x'_{\rm lim}]_{\Lambda{\rm CDM}}} = \frac{[r_{\rm lim}/r_{\rm vir}]_{\rm open}}{[r_{\rm lim}/r_{\rm vir}]_{\Lambda{\rm CDM}}} = \frac{[R_d(\rho_c(z)\Delta_c(z))^{\frac{1}{3}}]_{\rm open}}{[R_d(\rho_c(z)\Delta_c(z))^{\frac{1}{3}}]_{\Lambda{\rm CDM}}}. \tag{30}$$

Our calculation shows that the ratio is higher than 1. So, the resolved effect in the ΛCDM model is stronger than that in the open-CDM model for the same $M_{\rm vir}$.

Furthermore, galaxy clusters with high $M_{\rm vir}$ have low concentration parameters c and larger sizes. So corresponding to the same $x'_{\rm lim}$, $F(z, x'_{\rm lim})$ should be lower, i.e., more signal will be lost. Then the resolved effect will be stronger with high $M_{\rm vir}$.

We can also rewrite $x'_{\rm lim}$ as

$$x'_{\rm lim} = \frac{\theta_c}{\theta_{\rm vir}}, \tag{31}$$

where $\theta_{\rm vir} = r_{\rm vir}/R_d$ denotes the cluster's virial angular radius. Given $M_{\rm vir}$, $\theta_{\rm vir}$ decreases with increasing redshift z. Thus when z is high enough so that $\theta_{\rm vir}$ of the galaxy cluster is smaller than $\theta_{\rm c}$, the resolved count will merge to the unresolved count, which is consistent with our results.

To see the resolved effect in the two low$-\Omega_0$ models more directly, we plot the total number of SZE clusters N for different $S_\nu^{\rm lim}$ in Figs. 6 and 7. The results show that given $S_\nu^{\rm lim} < 10\,{\rm mJy}$, the resolved effect with $D = 1.2\,{\rm m}$ has little influence on the cluster count. For $S_\nu^{\rm lim} > 10$ mJy, $N(D = 1.2\,{\rm m})$ is markedly lower. At $S_\nu^{\rm lim} = 20$ mJy, $N(D = 2.5$ m) is about one third less than N(unresolved). With $D = 2.5$ m, $N(D = 2.5\,{\rm m})$ is drastically different from that of the unresolved case, about one-half lower than N(unresolved) at $S_\nu^{\rm lim} = 10\,{\rm mJy}$ and one order of magnitude lower at $S_\nu^{\rm lim} = 90\,{\rm mJy}$.

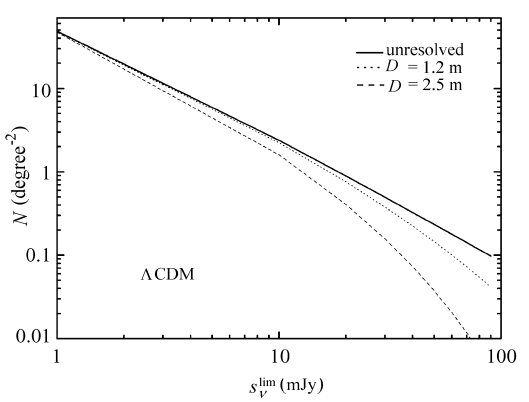

Fig. 6 Total number of SZE clusters corresponding to different $S_\nu^{\rm lim}$ for the ΛCDM model. The solid, dotted and dash line represents unresolved count and the resolved counts with $D = 1.2\,{\rm m}$ and $D = 2.5\,{\rm m}$, respectively.

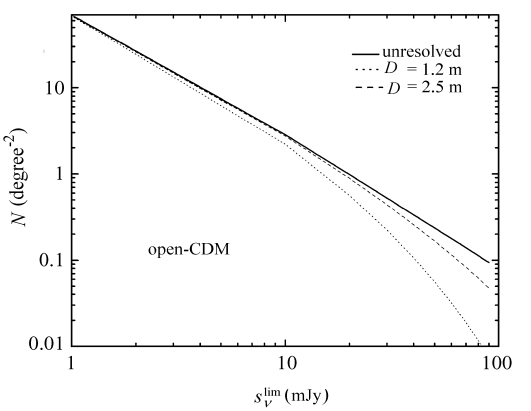

Fig. 7 Total number of SZE clusters corresponding to different $S_\nu^{\rm lim}$ for open-CDM model. The solid, dotted and dash line represents unresolved count and the resolved counts with $D = 1.2\,{\rm m}$ and $D = 2.5\,{\rm m}$, respectively.

From the above, we conclude that it is significant to check whether the resolved effect should be taken into account when making predictions for different SZ cluster surveys, especially for those with high $S_\nu^{\rm lim}$ or large D.

At present, there are several proposed or planned antenna arrays that will be used for surveying SZE clusters, such as AMIBA (Lo et al.), AMI (Kneissl et al. 2001) and SZA (Holder et al. 2000). We list their observing characteristics in Table 1.

It can be found that $\theta_{\rm cutoff}$ are relatively large. In addition, the sensitivities of these antenna arrays are high and $S_\nu^{\rm lim}$ can be as low as 5 mJy. So for these SZE surveys, the resolved effect would be negligible, and we can use the unresolved counts safely to predict the survey results for different cosmological models. We also should mention here that besides the resolved effects,

there are other issues needed to be considered in a real survey, and thus careful studies on a specific survey should be taken in order to give detailed predictions on the observational gains.

Table 1

	D(m)	Operating frequency (GHz)	$\theta_{\rm cutoff}$ (arcmin)
AMIBA	1.2	90	4.7
	0.3	90	18.9
AMI	13.0	15	3.8
	3.7	15	17.4
SZA	2.5	30	7.0

Appendix

Table A1

α	1.0	1.5
$y_{\rm DM}$	$\frac{1}{x(1+x)^2}$	$\frac{1}{x^{1.5}(1+x)^{1.5}}$
c	$6(\frac{M_{\rm vir}}{10^{14}\,h^{-1}\,M_\odot})^{-1/5}$	$3.529(\frac{M_{\rm vir}}{10^{14}\,h^{-1}\,M_\odot})^{-1/5}$
$[\ln\rho_{\rm gas}/\ln r_{\rm vir}]_{r_{\rm vir}}$	$\frac{1+3c}{1+c}$	$1.5\frac{1+2c}{1+c}$
$m(x)$	$\ln(1+x)-\frac{x}{1+x}$	$2\ln(\sqrt{x}+\sqrt{1+x})-2\sqrt{\frac{x}{1+x}}$
$\int_0^x du\frac{m(u)}{u^2}$	$1-\frac{\ln(1+x)}{x}$	$-\frac{2\ln(\sqrt{x}+\sqrt{1+x})}{x}+2\sqrt{\frac{1+x}{x}}$
$M(\le r)$	$[\frac{m(c\cdot r/r_{\rm vir})}{m(c)}]M_{\rm vir}$	$[\frac{m(c\cdot r/r_{\rm vir})}{m(c)}]M_{\rm vir}$

References

Bahcall N., Fan X., 1998, ApJ, 504, 1

Barbosa D., Bartlett J. G., Blanchard A., Oukbir J., 1996, A&A, 314, 13

Bartlett J. G., 2000, A&A, astro-ph/0001267

Benson A. J., Reichardt C., Kamionkowski M., 2002, MNRAS, 331, 71

Birkinshaw M., 1999, Physics Reports, 310, 97

Carlstrom J. E., Joy M., Grego Lo, Holder G., Holzapfel W. L., LaRoque S., Mohr J. J., Reese E. D., 2000, In Durret F., Gerbal G., astro-ph/0103480

Eke V. E., Navarro J. F., Frenk C. S., 1998, ApJ, 503, 569

Eke V. E., Cole S., Frenk C. S., 1996, ApJ, 282, 263

Fan Z., Chiueh T., 2001, ApJ, 550, 547

Holder G. P., Carlstrom J. E., 2001, ApJ, 558, 515

Holder G. P., Mohr J. J., Carlstrom J. E., Evrard A. E., Leitch E. M., 2000, ApJ, 544, 629

Jain B., Seljek U., 1997, ApJ, 484, 560

Jing Y. P., Suto Y., 2000, ApJ, 529, L69

Kneissl R., Jones M., Saunders R., Eke V. E., Lasenby A. N., Grainge K., Cotter G., 2001, MNRAS, 328, 783

Komatse E., Seljek U., 2001, MNRAS, 327, 1353
Lo K. Y., Chiueh T. H., Martin R. N., Ng K. W., Liang H., Pen U. l., Ma C. P., 2001, AIP, 586, 172
Makino N., Sasaki S., Suto Y., 1998, ApJ, 497, 555
Mohr J. J., Carlstrom J. E., Holder G. P., Holzapfel W. J., Joy M. K., Leitch E. M., Reese E. D., In: Jacqueline Bergeron, Alvio Renzini, eds., Proceedings of the ESO Symposium held at Antofagasta, From Extrasolar Planets to Cosmology: The VLT Opening Symposium, Berlin: Springer-Verlag, 2000, p.150
Mohr J. J., White S. D. M., 2002, MNRAS, 336, 112
Moore B., Governato F., Quinn T., Stadel J., Lake G., 1998, ApJ, 499, L5
Navarro J. F., Frenk C. S., White S. D. M., 1997, ApJ, 490, 493
Oukbir J., Bartlett J. G., Blanchard A., 1997, A&A, 320, 365
Press W. H., Schechter P., 1974, ApJ, 187, 425
Sunyaev R. A., Zel'dovich 1980, ARA&A, 18, 537
Suto Y., Sasaki S., Makino N., 1998, ApJ, 509, 544